

# Fractional topology in open systems

Xi Wu,<sup>1,\*</sup> Xiang Zhang,<sup>2,†</sup> and Fuxiang Li<sup>2,‡</sup>

<sup>1</sup>*School of Physics, Henan Normal University, Xinxiang 453007, China*

<sup>2</sup>*School of Physics and Electronics, Hunan University, Changsha 410082, China*

We investigate the emergence of fractional topological invariants in a periodic Su–Schrieffer–Heeger chain subject to gain and loss, governed by the Gorini–Kossakowski–Sudarshan–Lindblad master equations. After preparing the symmetry condition for integer topological invariants, we investigate their transition to fractional ones in steady states, which can happen either by tuning parameters in jump operators or as a dynamical transition during time evolution. Moreover, we show that these fractional topological invariants no longer possess quantized topology in the conventional sense. However, by extending the Brillouin zone to cover multiple cycles, the total winding regains integer quantization. Finally, we show how such effects can be observed in long-range hopping photonic lattices with fractional fillings, via Bloch state tomography. Our results open a new pathway to understand fractional topology in open quantum systems.

## I. INTRODUCTION

In recent decades, people have gradually drawn attention to the study of open systems[1–26] described by Gorini–Kossakowski–Sudarshan–Lindblad master equation(Lindblad master equation in short) [27–29]that governs the time evolution of density matrix

$$\frac{d\rho}{dt} = -i[H, \rho] + \sum_{\mu} (2L_{\mu}\rho L_{\mu}^{\dagger} - \{L_{\mu}^{\dagger}L_{\mu}, \rho\}) \equiv \mathcal{L}\rho, \quad (1)$$

where  $H = \sum_{ij} c_i^{\dagger} h_{ij} c_j$  is quadratic in terms of the fermionic creation (annihilation) operators  $c_i^{\dagger}$  ( $c_i$ ). Here,  $h_{ij}$  are the elements of matrix  $H$ , which denotes the Hamiltonian in the single-particle basis and  $L_{\mu}$ 's are the Lindblad dissipators describing quantum jumps due to coupling to the environment.  $\mathcal{L}$  is called the Liouvillian superoperator. Formal solutions were established[5, 6, 29], through the third quantization procedure, which makes the study in the cases without interactions straightforward. From Eq. (1) one can see that non-Hermiticity naturally arises in the Liouvillian superoperator.

Rapid growth was seen in the field of topology of non-Hermitian matrices in the past decade[30–42]. Exceptional points(EP) are considered as a key signal for fractional topological invariant. In open systems described by Lindblad equation, the dynamics is related with the damping matrix  $X$ , which can be regarded as a non-Hermitian Hamiltonian. Note that this is different from the post-selected Hamiltonian that was considered as the effective Hamiltonian[43]. A natural intuition is that EP also can be used as a mechanism for fractional topological invariant in Lindblad open systems.

However, there are several limitations of this EP approach: First, from a practical point of view, it is very difficult to engineer eigenstates of  $X$  in steady states through gain matrix. [44] shows that EPs of  $X$  may not reach steady states. Therefore, a fractional winding number does not appear in steady states even if EPs occur in  $X$ . Second, to generate this construction to include mixed states is challenging. For generic mixed states, the density matrix should be used to define the topological invariant and it is only expanded by right eigenstates of  $X$ , not the left eigenstates. The famous construction of fractional winding number, for non-Hermitian Su–Schrieffer–Heeger(NHSSH) model, through right states is done by Tony Lee, who considers the trajectory of momentum in  $\langle\sigma_x\rangle, \langle\sigma_z\rangle$  space[30], excluding  $\langle\sigma_y\rangle$  for no specific reason. The orbit of these expectation values in the Bloch sphere is not symmetric, making the total Berry phase non-topological.

Can we cook up a simple setup for fractional winding number in terms of Berry phase in open systems, which is also topological? EPs themselves are not the necessary condition for the fractional topological invariant. What is important is the multi-valueness of the physical states, which is also the essence of EP approach. Moreover, as we shall see the text below, at least in the NHSSH model, the parameter that induces EP in the eigenstates breaks the inversion symmetry, which keeps the Berry phase topological otherwise. The above concerns motivate us to take an alternative approach: we introduce the multi-valueness directly in the gain/loss matrix by a fractional momentum and keep the inversion symmetry in the Hamiltonian, gain/loss matrices and initial states. As a result, the above drawbacks can be overcome, and fractional winding numbers appear in the steady states. Based on our definition, our findings are as follows:

Under the symmetries required for quantization, single-valued gain and damping matrices guarantee that a completely filled lower band yields an integer winding number in the steady state; if the initial state is also single-valued, the winding number remains integer throughout the evolution. For fractional fillings, tuning the gain matrix drives the winding number away from

\* These authors contributed equally to this work.; [wuxi5949@gmail.com](mailto:wuxi5949@gmail.com)

† These authors contributed equally to this work.

‡ [fuxiangli@hnu.edu.cn](mailto:fuxiangli@hnu.edu.cn)

integrality. It can vary continuously and undergo abrupt jumps from integer to fractional values. These discontinuities occur when the purity gap closes, mirroring the mechanism of topological transitions in integer cases. In contrast to pure states in closed or non-Hermitian systems—where the winding numbers are rational—the values here depend sensitively on the structure of the states. Yet the topology survives in a re-quantized form: when the states exhibit  $n$  branches, the winding number defined over an  $n$ -period is strictly integer. We call this *multi-period re-quantization*, indicating that  $n$  Brillouin zones behave collectively as a single topological unit, insensitive to local details. Finally, the proposed model is experimentally accessible. In a 1D optical superlattice of ultracold fermions, the Berry phase of both steady and transient states can be directly probed.

## II. OUR MODEL

We will consider single particle loss and gain with loss dissipators  $L_\mu^l = \sum_i D_{\mu i}^l c_i$  and gain dissipators  $L_\mu^g = \sum_i D_{\mu i}^g c_i^\dagger$ , where  $D_{\mu i}$  are the complex coefficients. With the single-particle correlation[39, 45]  $\Delta_{ij}(t) = \text{Tr}[c_i^\dagger c_j \rho]$ , Eq. (1) can be recast as

$$\frac{d\Delta(t)}{dt} = X\Delta(t) + \Delta(t)X^\dagger + 2M_g \quad (2)$$

where the damping matrix

$$X = ih^T - M_l^T - M_g, \quad (3)$$

with  $(M_g)_{ij} = \sum_\mu D_{\mu i}^{g*} D_{\mu j}^g$  and  $(M_l)_{ij} = \sum_\mu D_{\mu i}^{l*} D_{\mu j}^l$ . Note that  $M_l$  and  $M_g$  are Hermitian matrices. The steady state correlation  $\Delta_s = \Delta(\infty)$ , to which long time evolution of any initial state converges, is determined by  $d\Delta_s/dt = 0$  or  $X\Delta_s + \Delta_s X^\dagger + 2M_g = 0$ . This equation is solved by:

$$\Delta_s = 2 \int_0^\infty e^{Xt} M_g e^{X^\dagger t} dt. \quad (4)$$

It can be seen that the steady state is determined by the gain matrix  $M_g$  and the damping matrix  $X$ . We present a simple model of open quantum system: a standard Su-Schrieffer-Heeger(SSH) model with single particle gain and loss with fractional momentum:  $H = \sum_{ij} h_{ij} c_i^\dagger c_j$  and  $L_\mu^g = L_{\mu i}^g c_i^\dagger$  and  $L_\mu^l = L_{\mu i}^l c_i$ . In momentum space,  $L_1^g(k) = \sqrt{\gamma_1}(c_A^\dagger + c_B^\dagger)$ ,  $L_2^g(k) = \sqrt{\gamma_2}(c_A^\dagger e^{-ik/n} + c_B^\dagger)$ ,  $L_3^g(k) = \sqrt{\gamma_0}c_A^\dagger$ ,  $L_4^g(k) = \sqrt{\gamma_0}c_B^\dagger$ ,  $L_1^l(k) = \sqrt{\gamma_1}(c_A - c_B)$ ,  $L_2^l(k) = \sqrt{\gamma_2}(c_A e^{-ik/n} - c_B)$ ,  $L_3^l(k) = \sqrt{\gamma_0}(c_A + ic_B)$ . For concreteness we choose  $n = 3$  without loss of generality. Then the damping matrix  $X$

and the gain matrix  $M_g(k)$  read

$$X(k) = i [(t_1 + t_2 \cos k)\sigma_x + t_2 \sin k \sigma_y] - \Gamma \sigma_0 \quad (5)$$

$$M_l = (\gamma_1 + \gamma_2)\sigma_0 - (\gamma + \cos \frac{k}{3})\sigma_x - \sin \frac{k}{3}\sigma_y \quad (6)$$

$$M_g = (\gamma_1 + \gamma_2)\sigma_0 + (\gamma + \cos \frac{k}{3})\sigma_x + \sin \frac{k}{3}\sigma_y. \quad (7)$$

where  $\Gamma = \gamma_1 + \gamma_2$  which is also called the Liouvillian gap, governing the relaxation of the open quantum system. For simplicity, we set  $\gamma_1 = \gamma_2 = 0.5$  as follows. In general, the Liouvillian gap  $\Gamma$  is less than 0, ensuring the existence of the steady state. It can also be seen that the concrete form of the damping matrix does not contain the control parameter  $\gamma$ .

We define our topological winding number through the following procedure: First we map the mixed state density matrices into the corresponding pure state density matrices[46] with the same solid angle in the Bloch sphere, dubbed the directional purification procedure

$$\rho \xrightarrow{\text{same solid angle}} P = |\psi\rangle\langle\psi|; \quad (8)$$

Second, we use the standard Berry phase to define the topological winding number:

$$N = \frac{\Phi}{\pi} = \frac{-i}{\pi} \int_0^{2\pi} \langle\psi| \frac{\partial}{\partial k} |\psi\rangle dk \quad (9)$$

$$= \frac{1}{4\pi} \int_S \epsilon_{ijk} \hat{\rho}_i d\hat{\rho}_j \wedge d\hat{\rho}_k, \quad (10)$$

where  $S$  is the area whose boundary is the trajectory of  $\hat{\rho}_i(k) = \text{Tr} P \sigma_i$ , which can also be calculated by  $\hat{\rho}_i(k) = \rho_i(k) / \sqrt{\sum_j \rho_j^2}$  where  $\rho_i(k) = \text{Tr} \rho \sigma_i$ . There are three advantages of this definition: first, the solid angle is preserved among the density matrix, the correlation matrix and the modular Hamiltonian, which validates our fractional winding number as a unique result(See supplementary material B); second, it can be easily read out via the trajectory of  $\langle\sigma_x\rangle, \langle\sigma_y\rangle, \langle\sigma_z\rangle$  in the Bloch sphere; third, it has a corresponding observable in the coordinate space as the ensemble geometric phase in the thermodynamic limit[47].

The chiral symmetry is usually broken during the time evolution in open systems except when the Hamiltonian itself is too trivial[48, 49]. In order to discuss more interesting physics from the SSH model Hamiltonian, we ignore the chiral symmetry but consider the inversion symmetry [50],

$$\sigma_1 \mathcal{O}(k) \sigma_1 = \mathcal{O}(-k), \quad \mathcal{O} = X, M_{g/l}, \Delta(t=0, k), \quad (11)$$

which gives

$$\sigma_1 \Delta(t, k) \sigma_1 = \Delta(t, -k). \quad (12)$$

during the evolution(See Supplementary material A for details). Our choice of  $X, M_{g/l}$  and eigenstate of  $X$

as the initial state obey this symmetry. Eq. (12) can be expressed by  $\sigma$  averages  $\hat{\delta}_i = \delta_i / \sum_j \delta_j^2$  where  $\delta_a = \text{Tr}(\Delta\sigma_a)$   $i = 1, 2, 3$  as

$$\hat{\delta}_1(k) = \hat{\delta}_1(-k) \quad (13)$$

$$\hat{\delta}_{2,3}(k) = -\hat{\delta}_{2,3}(-k). \quad (14)$$

The Berry phase is half the area whose contour is given

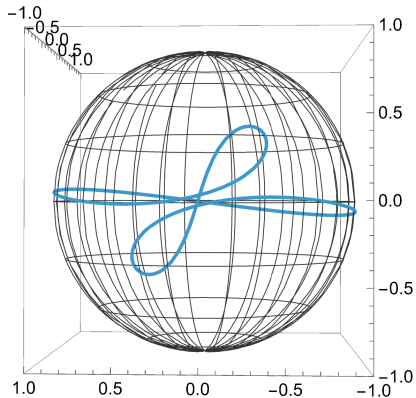


Figure 1. The trajectory of  $\hat{\delta}_i(k)$  on the Bloch sphere, symmetric about  $k = 0$  and  $k = 3\pi$ , divides the surface into two equal parts.

by the trajectory of  $\hat{\delta}_i(k)$  in Fig. 6. The inversion symmetry is visualized as an axis symmetry in the sphere, that is, a  $\pi$  rotation around  $x$ -axis which makes this contour unchanged. Therefore, the area above this contour is the same as the area below this contour, making them both  $0$  or  $2\pi$ . So the Berry phase is quantized as  $0$  or  $\pi$  for a complete filled lower band. However, a parameter as a real coefficient in front of  $\sigma_2$  in Eq. (5), giving rise to EPs in  $X$ , breaks this symmetry.

### III. THE CONDITION FOR INTEGER WINDING NUMBER

If  $X$  and  $M_{g/l}$  are single-valued matrices in the Brillouin zone, that is,  $X(k + 2\pi) = X(k)$ ,  $M_{g/l}(k + 2\pi) = M_{g/l}(k)$ , then the winding number is an integer. Let us first prove it for steady states. The steady state correlation matrix can be expanded by Pauli matrices with coefficients:

$$\delta_a^s = \text{Tr}(\Delta_s \sigma_a), \quad a = 0, 1, 2, 3. \quad (15)$$

Eq. (3) shows that we can deform  $M_g$  &  $M_l^T$  s.t.  $X$  remains completely unchanged, so  $M_g$  and  $X$  are independent.  $\text{Tr}(e^{Xt} M_g e^{X^\dagger t} \sigma_i)$  is always finite. So

$$\delta_i^s = \text{Tr}(\Delta_s \sigma_i) \equiv 2 \int_0^\infty \text{Tr}(e^{Xt} M_g e^{X^\dagger t} \sigma_i) dt.$$

But  $\text{Tr}(e^{Xt} M_g e^{X^\dagger t} \sigma_i)(k + 2\pi) = \text{Tr}(e^{Xt} M_g e^{X^\dagger t} \sigma_i)(k)$ . Since the integrand is finite,  $\delta_i^s$  is also single-valued as  $M_g$ :

$$\delta_i^s(k + 2\pi) = \delta_i^s(k). \quad (16)$$

Under the symmetries required for quantization,  $\delta_i(k)$ s can only wind integer times around the Bloch sphere when the Brillouin zone is covered. The proof is complete for steady states. For transient states,

$$\Delta(t) = e^{Xt} \tilde{\Delta}(0) e^{X^\dagger t} + \Delta_s,$$

we just need to add the presumption that  $\Delta(0)$  or  $\tilde{\Delta}(0)$  is single-valued and then the proof is completely parallel. The appearance of exceptional points in the non-Hermitian damping matrix  $X$ , though gives multi-valued eigenvalues and eigenvectors, does not change the single-valuedness of matrix  $X$  itself. Therefore, exceptional points are not the sufficient condition for the fractional winding number of generic mixed states in Lindblad open systems. The proof for steady states also explains why EPs lie away from steady states[44]. Moreover, our analysis does not depend on the dimension of Brillouin zone and for multi-band systems, replacing  $\sigma_a$  with  $SU(N)$  generators  $\lambda_a$  does not change the logic. A simple way to introduce fractional winding number is to expand the periodicity in  $M_{g/l}$  by  $M_{g/l}(k + 2n\pi) = M_{g/l}(k)$  with  $n > 1$ , which is our construction.

### IV. TOPOLOGICAL PHASE TRANSITIONS BEYOND THE INTEGER REALM

We show examples in 3-period re-quantization, in steady states and transient states. The phase transition occurs at  $M_g(k_0) \propto M_l^T(-k_0)$  for steady states and  $\frac{d}{dt}(e^{Xt} \tilde{\Delta}(0) e^{X^\dagger t}) = (2 - c)M_g(k_0) - cM_l^T(-k_0)$  for transient states at some momenta  $k_0$ s,  $c$  being a constant(See C for details). We have checked that once  $M_g$  is fixed, tuning parameter, which gives exceptional points(EP) in the damping matrix  $X$ , does not induce a topological phase transition in the steady state. So, the 3-branch structure does not necessarily come from EPs of  $X$ . For transient states, the winding number may have fractional values in special choices of the parameters and jump during the phase transition. As a result of general states with multi-valuedness of mappings on momentum space, perfect fractional winding number is not protected, even for a pure state that is a linear combination of eigenstates of a non-Hermitian Hamiltonian.

#### A. Fractional topological phase transitions of steady state

Before studying the dynamical phase transitions, we need to understand the topology of the steady state.

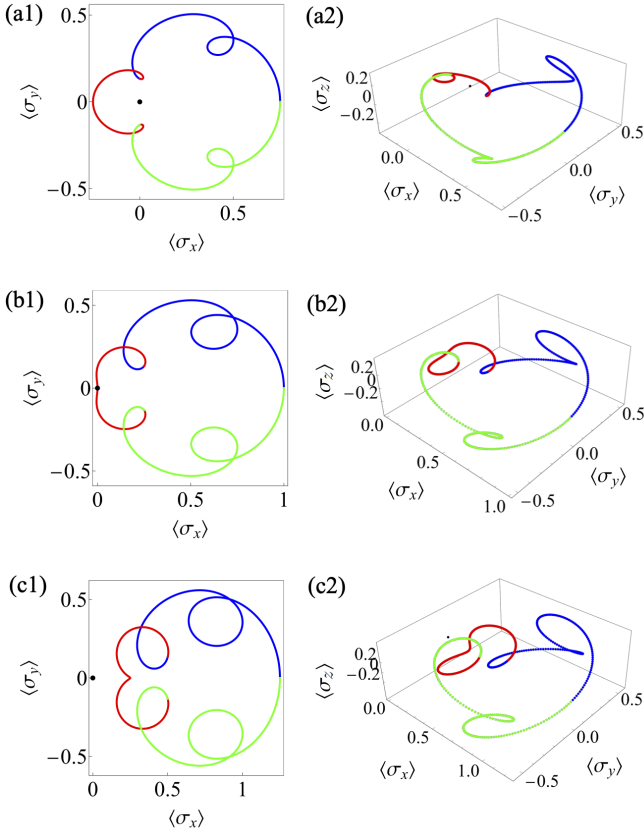


Figure 2. Topological phase transitions of nonequilibrium steady state in SSH model for period  $6\pi$ . Blue, red, and green lines correspond to period  $2\pi$ . Steady state is determined by  $M_g$  (Eq. 7).  $\gamma = 0.5, 1, \text{ and } 1.5$  for (a1), (b1), and (c1). (a2)-(c2) are the three-dimensional trajectory of  $\langle\sigma_x\rangle(t)$ ,  $\langle\sigma_y\rangle(t)$  and  $\langle\sigma_z\rangle(t)$ .

From Eq. (4), the steady state is fully determined by the gain matrix  $M_g$ . Incorporating with Eq. (7), we reveal that the control parameter  $\gamma$  can drive the steady state phase transitions, as shown in Fig. 2. In Fig. 2, we show that the steady state  $C_s$  is topological for  $\gamma < 1$  and trivial for  $\gamma > 1$ , corresponding to the winding number  $\nu = 1$  and  $\nu = 0$  under the momentum period of  $6\pi$ . Therefore, the topological invariant is remarkably fractional for  $\gamma < 1$  if we only consider  $2\pi$  period. At the critical point  $\gamma = 1$ , the trajectory of  $(\langle\sigma_x\rangle, \langle\sigma_y\rangle)$  cross the origin point, indicating the occurrence of topological phase transitions of the steady state. The blue, red and green curves correspond to the momentum period of  $[0, 2\pi]$ ,  $[2\pi, 4\pi]$  and  $[4\pi, 6\pi]$ .

### B. Fractional dynamical phase transitions

We now begin to investigate the dynamical phase transitions wherein the topological invariant undergoes non-trivial changes during time evolution. The main results are shown in Fig. 3. In the upper panels, we show the

winding numbers of  $(\langle\sigma_x\rangle(t), \langle\sigma_y\rangle(t))$  at different times under the  $6\pi$  momentum periods. For comparison, we also present the 3D winding of  $(\langle\sigma_x\rangle(t), \langle\sigma_y\rangle(t), \langle\sigma_z\rangle(t))$  in the lower panels. In stark contrast to the previous studies [48, 49], we reveal a *Integer to Fraction* dynamical phase transitions. At time  $t = 0$ , the initial state is the eigenstate of the damping matrix  $X$  and the winding number is  $\nu = 1$  under  $2\pi$  momentum period, as demonstrated in the Fig. 3 (a). Note that the trajectory of blue, red and green lines overlap with each other. As the system evolves, the winding number undergoes a topological phase transitions from Fig. 3 (b) to Fig. 3 (c). Interestingly, the winding number of this topological phase transitions is changed from integer to fraction if we focus on  $2\pi$  period. Although the winding number of Fig. 3 (c) is not a perfect fraction  $1/3$ , the winding number is recovered to an integer  $\nu = 1$  when the momentum period is extended to  $6\pi$ .

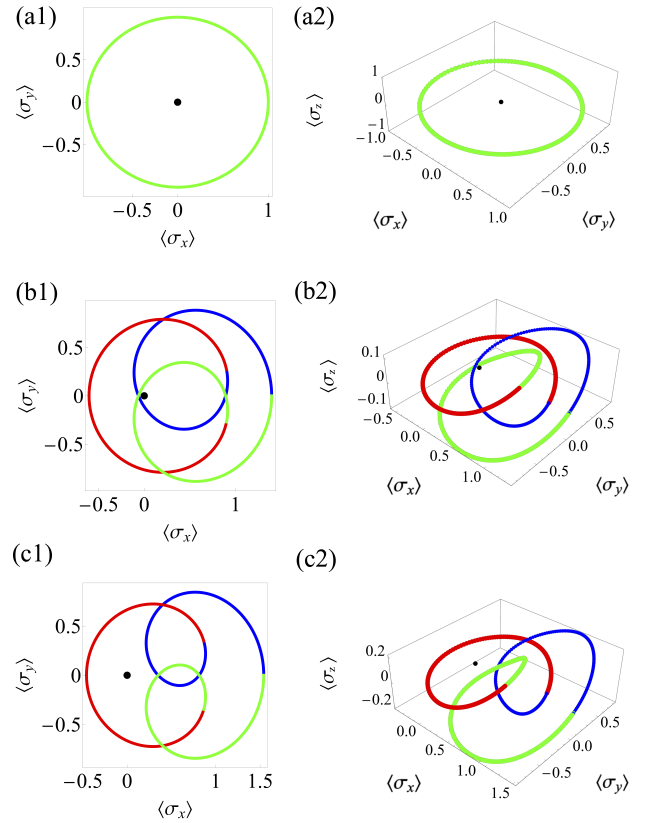


Figure 3. Dynamical phase transitions in SSH model. Integer topological invariants to fractional topological invariants. (a1)-(c1) are the trajectory of  $\langle\sigma_x\rangle(t)$  and  $\langle\sigma_y\rangle(t)$ , corresponding to time  $t = 0, t = 0.1, t = 0.2$ , and nonequilibrium steady state, respectively. (a2)-(c2) are the three-dimensional trajectory of  $\langle\sigma_x\rangle(t)$ ,  $\langle\sigma_y\rangle(t)$  and  $\langle\sigma_z\rangle(t)$ . Here,  $t_1 = 1, t_2 = 2, \gamma_1 = \gamma_2 = 0.5$  and  $\gamma = 1.2$ . Under this setting, the steady state is topological trivial, corresponding to Fig. 2 (c1).

### C. Fractional winding number 1/3

By tuning  $\gamma$ , an exact fractional winding number 1/3 can be achieved. Taking advantage of the inversion symmetry allows this to be done easily. Actually, the angle in the  $\langle\sigma_x\rangle$   $\langle\sigma_y\rangle$  plane can determine the  $\pi/6$  Berry phase which is the 1/3 winding number very well. We focus on the momentum period  $[2\pi, 4\pi]$  which is the red curve. By tuning  $\gamma$  such that its projection covers the angle  $2\pi/3$  in the  $\langle\sigma_x\rangle$   $\langle\sigma_y\rangle$  plane, the red curve together with the north/south pole in the Bloch sphere in  $\langle\sigma_x\rangle$   $\langle\sigma_y\rangle$   $\langle\sigma_z\rangle$  also covers the solid angle  $2\pi/3$  because of the  $\pi$  rotation axis symmetry in the sphere.

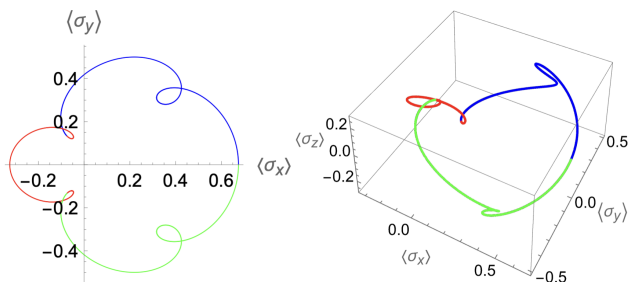


Figure 4. The left figure is the trajectory of  $\langle\sigma_x\rangle$  and  $\langle\sigma_y\rangle$ , and nonequilibrium steady state. The right figure is the three-dimensional trajectory of  $\langle\sigma_x\rangle$ ,  $\langle\sigma_y\rangle$  and  $\langle\sigma_z\rangle$ . Here,  $t_1 = 1$ ,  $t_2 = 2$ ,  $\gamma_1 = \gamma_2 = 0.5$  and  $\gamma = 0.35$ . The steady state has winding number 1/3.

## V. EXPERIMENTAL OBSERVABLES AND SETUPS

For usual local models and dissipation, fractional momentum may not arise.  $M_g(k)$  of Eq. (7) in coordinate space may involve highly nonlocal dissipation which is not easy to engineer. Here we give a resolution via simulation: One can consider another model that has a similar structure

$$H'(k) = (t_1 + t_3 \cos(3k)) \sigma_1 + t_3 \sin(3k) \sigma_2 \quad (17)$$

$$M'_g(k) = \mathbb{I} + \cos(k) \sigma_1 + \sin(k) \sigma_2. \quad (18)$$

with  $K = 3k$  such that

$$H(K) = (t_1 + t_3 \cos K) \sigma_1 + t_3 \sin K \sigma_2 \quad (19)$$

$$M_g(K) = \mathbb{I} + \cos\left(\frac{K}{3}\right) \sigma_1 + \sin\left(\frac{K}{3}\right) \sigma_2. \quad (20)$$

The true momentum is  $k \in [0, 2\pi)$  so  $K \in [0, 6\pi)$ . In order to simulate the same topology, one fills only 1/3 of the lower band s.t.  $k \in [0, 2\pi/3)$ , then  $K \in [0, 2\pi)$ . In  $K$  space,  $H(K)$  indeed has the periodicity  $2\pi$  and  $M_g(K)$  has multiplicity three in  $2\pi$ . Model Eq. (17) can be realized by long-range hopping, see Fig. (5). The exact 1/3 filling fraction can be guaranteed in the setup when

the initial state, as an eigenstate of  $H'(k)$ , has a winding number 1. Then one can find that fractional winding number appears at the steady states. Multi-period re-quantization appears naturally as the lower band is completely filled.

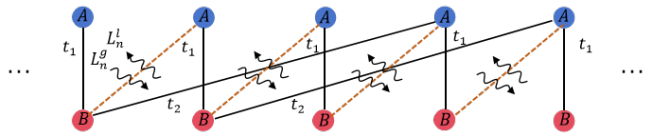


Figure 5. Sketch of the generalized Su-Schrieffer-Heeger model with long-range hopping. Solid lines represent the intra-cell hopping  $t_1$  between  $(n, A)$  and  $(n, B)$  and the inter-cell hopping  $t_2$  between  $(n, B)$  and  $(n+3, A)$ . Dashed lines are the fermion loss and gain, described by the dissipators  $L_n^l$  and  $L_n^g$ .

The proposed model can be implemented in a 1D optical superlattice using ultracold fermionic atoms (e.g.  $^{40}\text{K}$  or  $^6\text{Li}$ ) confined in optical potentials. A tunable SSH-type configuration is realized via staggered tunneling amplitudes  $t_1$  and  $t_2 = 0$  controlled by adjusting the relative intensities and phases of the two standing-wave laser fields forming the superlattice [51]. An additional Raman-assisted tunneling is introduced to couple sites  $A(n)$  and  $B(n+3)$ , thereby generating the long-range hopping amplitude  $t_3$ . This can be implemented by introducing a momentum transfer  $3(2\pi/a)$  through a two-photon Raman process [52, 53]. The amplitude and phase of  $t_3$  are controlled by the Raman intensity and detuning, allowing precise tuning of the effective Hamiltonian.

A direct observation can be accessed via standard Bloch state tomography [54–57], which has been used to probe topology in quench dynamics. One just needs to measure  $\rho_i(t, k) = \text{Tr} \rho(t, k) \sigma_i$  or  $\delta_i(t, k) = \text{Tr} \Delta(t, k) \sigma_i$ , being aware that  $\sigma_i$  is not the true spin but a pseudo spin coming from the two-band structure, and plot the trajectory of them in the Bloch sphere for each time  $t$  as it evolves.

## ACKNOWLEDGEMENTS

X Wu thank Prof. Yan He and Prof. Keyu Su for invaluable discussions.

### Appendix A: Inversion symmetry during time evolution

In this section, we show that inversion symmetry protect the quantized value  $\pi$  of Berry phase in Lindblad open systems, generalizing the result in quench dynamics in [50]. Inversion symmetry can be expressed for opera-

tors as:

$$\sigma_1 X(k) \sigma_1 = X(-k) \quad (\text{A1})$$

$$\sigma_1 M_g(k) \sigma_1 = M_g(-k) \quad (\text{A2})$$

$$\sigma_1 \Delta(0, k) \sigma_1 = \Delta(0, -k) \quad (\text{A3})$$

where  $\Delta(0, k)$  is the single-particle correlation in the initial state.

The proof can be done in three steps: first, we show the equivalence of inversion symmetry in the correlation matrix and that in the modular Hamiltonian; second, we prove that the inversion symmetry is preserved in the correlation function during the time evolution and in the steady states; third, we show that based on the inversion symmetry, the Berry phase is quantized.

The relation between the correlation function  $\Delta$  and the modular Hamiltonian  $K$  is

$$\Delta = \frac{1}{e^{K^T} + 1} \Leftrightarrow K^T = \ln(\Delta^{-1} - 1). \quad (\text{A4})$$

Then the following expressions

$$\sigma_1 \Delta \sigma_1 = \frac{1}{e^{\sigma_1 K^T \sigma_1} + 1}, \quad (\text{A5})$$

$$\sigma_1 K^T \sigma_1 = \ln((\sigma_1 \Delta \sigma_1)^{-1} - 1) \quad (\text{A6})$$

validate the equivalence of inversion symmetry in two matrices

$$\sigma_1 \Delta(k) \sigma_1 = \Delta(-k) \Leftrightarrow \sigma_1 K(k) \sigma_1 = K(-k). \quad (\text{A7})$$

Next, we prove

$$\sigma_1 \Delta(t, k) \sigma_1 = \Delta(t, -k). \quad (\text{A8})$$

From Eq.(A1) Eq. (A2) ,

$$\begin{aligned} \sigma_1 \Delta_s(k) \sigma_1 &= 2\sigma_1 \int_0^\infty e^{X(k)t} M_g(k) e^{X^\dagger(k)t} dt \sigma_1, \\ &= 2 \int_0^\infty e^{X(-k)t} M_g(-k) e^{X^\dagger(-k)t} dt = \Delta_s(-k). \end{aligned} \quad (\text{A9})$$

From Eq. (A3) and

$$\Delta(0, k) = \tilde{\Delta}(0, k) + \Delta_s(k), \quad (\text{A10})$$

we have

$$\sigma_1 \tilde{\Delta}(0, k) \sigma_1 = \tilde{\Delta}(0, -k). \quad (\text{A11})$$

Therefore,

$$\begin{aligned} \sigma_1 \Delta(t, k) \sigma_1 &= \sigma_1 e^{X(k)t} \tilde{\Delta}(0, k) e^{X^\dagger(k)t} \sigma_1 + \sigma_1 \Delta_s(k) \sigma_1 \\ &= e^{X(-k)t} \tilde{\Delta}(0, -k) e^{X^\dagger(-k)t} + \Delta_s(-k) \\ &= \Delta(t, -k). \end{aligned} \quad (\text{A12})$$

Last, we show the quantization of Berry phase. Eq.(A8) can be expressed by  $\sigma$  averages  $\delta_a = \text{Tr}(\Delta \sigma_a)$  as

$$\delta_{0,1}(k) = \delta_{0,1}(-k) \quad (\text{A13})$$

$$\delta_{2,3}(k) = -\delta_{2,3}(-k). \quad (\text{A14})$$

Then for  $\hat{\delta}_i = \delta_i / \delta_j^2$  where  $i = 1, 2, 3$  we have

$$\hat{\delta}_1(k) = \hat{\delta}_1(-k) \quad (\text{A15})$$

$$\hat{\delta}_{2,3}(k) = -\hat{\delta}_{2,3}(-k). \quad (\text{A16})$$

The Berry phase is half the area whose contour is given

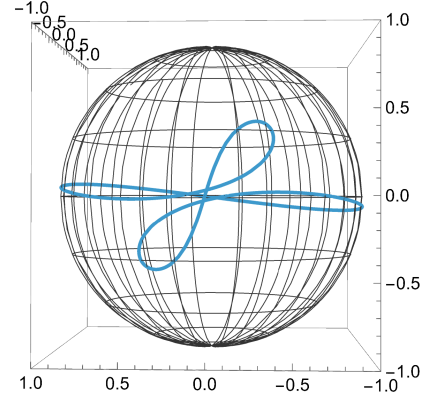


Figure 6. The trajectory of  $\hat{\delta}_i(k)$  on the Bloch sphere, symmetric about  $k = 0$  and  $k = \pi$ , divides the surface into two equal parts.

by the trajectory of  $\hat{\delta}_i(k)$  in Fig. 6. The inversion symmetry is translated into a central symmetry in the sphere, that is, a  $\pi$  rotation around  $x$ -axis which makes this contour unchanged. Therefore, the area above this contour is the same as the area below this contour, making them both  $2\pi$ . So the Berry phase is quantized as  $\pi$ .

### Appendix B: Solid angle is preserved between the correlation function, the modular Hamiltonian and the density matrix

The fact that angle is preserved among the correlation function  $\delta$ , the modular Hamiltonian  $K$ , and the density matrix  $\rho$  validates the uniqueness of our construction of fractional winding number. In the following we prove a more generic result: let  $F = f(\Delta)$  be a matrix function of  $\Delta$ , then

$$\hat{F}_i = \hat{\delta}_i, i = 1, 2, 3 \quad (\text{B1})$$

where  $\hat{F}_i = \frac{F_i}{|F|}$ ,  $F_i = \frac{1}{2} \text{Tr}(F \sigma_i)$ ,  $\hat{\delta}_i = \frac{\delta_i}{|\delta|}$ ,  $\delta_i = \frac{1}{2} \text{Tr}(\Delta \sigma_i)$ . This result tells us that the matrix function operation does not change the solid angle of a matrix  $\sigma$  average, which is the essence of the Berry phase.

Proof: Define

$$\bar{\Delta} := \Delta - \delta_0 \mathbb{I}, \bar{\Delta}^2 = |\bar{\delta}|^2 \mathbb{I} \quad (\text{B2})$$

For simplicity we denote  $f(\Delta)$  by  $f(\bar{\Delta})$

$$F = f(\bar{\Delta}) = f_{\text{even}}(\bar{\Delta}) + f_{\text{odd}}(\bar{\Delta}), \quad (\text{B3})$$

$$\text{where } \begin{cases} f_{\text{even}}(\bar{\Delta}) = \frac{f(\bar{\Delta}) + f(-\bar{\Delta})}{2} \\ f_{\text{odd}}(\bar{\Delta}) = \frac{f(\bar{\Delta}) - f(-\bar{\Delta})}{2} \end{cases} \quad (\text{B4})$$

We then take a Taylor expansion

$$f(\bar{\Delta}) = \sum_{n=0}^{\infty} \frac{\bar{\Delta}^n}{n!} f^{(n)}(0) \quad (\text{B5})$$

and get

$$\begin{aligned} f_{\text{even}}(\bar{\Delta}) &= \sum_{n=0}^{\infty} \frac{\bar{\Delta}^{2n}}{(2n)!} f^{(2n)}(0) = f_{\text{even}}(\sqrt{\bar{\Delta}^2}) \quad (\text{B6}) \\ f_{\text{odd}}(\bar{\Delta}) &= \sum_{n=0}^{\infty} \frac{\bar{\Delta}^{2n+1}}{(2n+1)!!} f^{(2n+1)}(0) \\ &= \sum_{n=0}^{\infty} \frac{\sqrt{\bar{\Delta}^2}^{2n+1}}{(2n+1)!!} f^{(2n+1)} \frac{\bar{\Delta}}{\sqrt{\bar{\Delta}^2}} \\ &= f_{\text{odd}}(\sqrt{\bar{\Delta}^2}) \frac{\bar{\Delta}}{|\bar{\delta}|} \quad (\text{B7}) \end{aligned}$$

so

$$f(\bar{\Delta}) = f_{\text{even}}(\sqrt{\bar{\Delta}^2}) + f_{\text{odd}}(\sqrt{\bar{\Delta}^2}) \frac{\bar{\Delta}}{|\bar{\delta}|}. \quad (\text{B8})$$

Next we take  $\sigma$ -averages on both side of Eq. (B8) and get

$$F_i = \frac{f_{\text{odd}}(\bar{\Delta})}{|\bar{\delta}|} \delta_i. \quad (\text{B9})$$

Using the definition of  $\hat{F}_i$  and  $\hat{\delta}_i$  we finally arrive at Eq. (B1).

## Appendix C: Topological phase transition point

Topological phase transition for steady states occurs at

$$M_g(k) \propto X(k) + X^\dagger(k) = M_g(k) + M_l^T(-k) \quad (\text{C1})$$

$$\Leftrightarrow M_g(k) \propto M_l^T(-k) \quad (\text{C2})$$

This can be checked as following

$$\begin{aligned} \Delta_s(k) &= 2 \int_0^\infty e^{Xt} M_g e^{X^\dagger t} dt \\ &\propto \int_0^\infty e^{Xt} (X(k) + X^\dagger(k)) e^{X^\dagger t} dt \\ &= \int_0^\infty (e^{Xt} d(Xt) e^{X^\dagger t} + e^{Xt} e^{X^\dagger t} d(X^\dagger t)) \\ &= \int_0^\infty d e^{Xt} \cdot e^{X^\dagger t} + e^{Xt} d e^{X^\dagger t} \\ &= \int_0^\infty d (e^{Xt} \cdot e^{X^\dagger t}) = (e^{Xt} e^{X^\dagger t}) \Big|_{t=0}^{t=\infty} = -\mathbb{I}(\mathbb{B3}) \end{aligned}$$

meaning the steady state becomes completely mixed at momentum  $k$ . Dynamical topological phase transition occurs at

$$\frac{d}{dt} (e^{X(k)t} \tilde{\Delta}(0, k) e^{X^\dagger(k)t}) - 2M_g(k) \propto X(k) + X^\dagger(k) \quad (\text{C4})$$

This can be shown as following

$$\frac{d}{dt} \Delta(t) = X \Delta(t) + \Delta(t) X^\dagger + 2M_g \quad (\text{C5})$$

$$\Leftrightarrow \frac{d}{dt} \Delta(t) - 2M_g = X \Delta(t) + \Delta(t) X^\dagger \quad (\text{C6})$$

At dynamical topological phase transition

$$\Delta(t, k) \propto \mathbb{I}(k) \quad (\text{C7})$$

so

$$\frac{d}{dt} \Delta(t) - 2M_g \propto X + X^\dagger \quad (\text{C8})$$

combining with

$$\Delta(t) = e^{Xt} \tilde{\Delta}(0) e^{X^\dagger t} + \Delta_s \quad (\text{C9})$$

$$\frac{d}{dt} \Delta_s = 0 \quad (\text{C10})$$

we get Eq. (C4).

- 
- [1] Heinz-Peter Breuer and Francesco Petruccione. *The theory of open quantum systems*. OUP Oxford, 2002.
- [2] Berislav Buča and Tomaž Prosen. A note on symmetry reductions of the lindblad equation: transport in constrained open spin chains. *New Journal of Physics*, 14(7):073007, 2012.

- [3] Berislav Buča, Cameron Booker, Marko Medenjak, and Dieter Jaksch. Bethe ansatz approach for dissipation: exact solutions of quantum many-body dynamics under loss. *New Journal of Physics*, 22(12):123040, 2020.
- [4] Daniel Manzano. A short introduction to the Lindblad master equation. *AIP Advances*, 10(2):025106, 02 2020.

- [5] Tomaž Prosen. Third quantization: a general method to solve master equations for quadratic open fermi systems. *New Journal of Physics*, 10(4):043026, 2008.
- [6] Tomaž Prosen. Spectral theorem for the lindblad equation for quadratic open fermionic systems. *Journal of Statistical Mechanics: Theory and Experiment*, 2010(07):P07020, 2010.
- [7] M. Höning, M. Moos, and M. Fleischhauer. Critical exponents of steady-state phase transitions in fermionic lattice models. *Phys. Rev. A*, 86:013606, Jul 2012.
- [8] Juan Mauricio Torres. Closed-form solution of lindblad master equations without gain. *Phys. Rev. A*, 89:052133, May 2014.
- [9] Jan Carl Budich and Sebastian Diehl. Topology of density matrices. *Phys. Rev. B*, 91:165140, Apr 2015.
- [10] Nobuyuki Okuma and Masatoshi Sato. Quantum anomaly, non-hermitian skin effects, and entanglement entropy in open systems. *Phys. Rev. B*, 103:085428, Feb 2021.
- [11] A. McDonald, R. Hanai, and A. A. Clerk. Nonequilibrium stationary states of quantum non-hermitian lattice models. *Phys. Rev. B*, 105:064302, Feb 2022.
- [12] Makio Kawasaki, Ken Mochizuki, and Hideaki Obuse. Topological phases protected by shifted sublattice symmetry in dissipative quantum systems. *Phys. Rev. B*, 106:035408, Jul 2022.
- [13] Lukas Wawer and Michael Fleischhauer. Chern number and berry curvature for gaussian mixed states of fermions. *Phys. Rev. B*, 104:094104, Sep 2021.
- [14] Fei Yang, Zheng Wei, Xianqi Tong, Kui Cao, and Su-Peng Kou. Symmetry classes of dissipative topological insulators with edge dark states. *Phys. Rev. B*, 107:165139, Apr 2023.
- [15] Lucas Sá, Pedro Ribeiro, and Tomaž Prosen. Symmetry classification of many-body lindbladians: Tenfold way and beyond. *Phys. Rev. X*, 13:031019, Aug 2023.
- [16] O. Viyuela, A. Rivas, and M. A. Martin-Delgado. Uhlmann phase as a topological measure for one-dimensional fermion systems. *Phys. Rev. Lett.*, 112:130401, Apr 2014.
- [17] Mariya V. Medvedyeva, Fabian H. L. Essler, and Tomaž Prosen. Exact bethe ansatz spectrum of a tight-binding chain with dephasing noise. *Phys. Rev. Lett.*, 117:137202, Sep 2016.
- [18] Simon Lieu, Max McGinley, and Nigel R. Cooper. Tenfold way for quadratic lindbladians. *Phys. Rev. Lett.*, 124:040401, Jan 2020.
- [19] Simon Lieu, Ron Belyansky, Jeremy T. Young, Rex Lundgren, Victor V. Albert, and Alexey V. Gorshkov. Symmetry breaking and error correction in open quantum systems. *Phys. Rev. Lett.*, 125:240405, Dec 2020.
- [20] Masaya Nakagawa, Norio Kawakami, and Masahito Ueda. Exact liouvillian spectrum of a one-dimensional dissipative hubbard model. *Phys. Rev. Lett.*, 126:110404, Mar 2021.
- [21] Wei Nie, Mauro Antezza, Yu-xi Liu, and Franco Nori. Dissipative topological phase transition with strong system-environment coupling. *Phys. Rev. Lett.*, 127:250402, Dec 2021.
- [22] A. McDonald and A. A. Clerk. Exact solutions of interacting dissipative systems via weak symmetries. *Phys. Rev. Lett.*, 128:033602, Jan 2022.
- [23] Emma C. King, Johannes N. Kriel, and Michael Kastner. Universal cooling dynamics toward a quantum critical point. *Phys. Rev. Lett.*, 130:050401, Feb 2023.
- [24] Kohei Kawabata, Ramanjit Sohal, and Shinsei Ryu. Lieb-schultz-mattis theorem in open quantum systems. *Phys. Rev. Lett.*, 132:070402, Feb 2024.
- [25] Clemens Gneiting, Akshay Koottandavida, A. V. Rozhkov, and Franco Nori. Unraveling the topology of dissipative quantum systems. *Phys. Rev. Res.*, 4:023036, Apr 2022.
- [26] Christian Leefmans, Avik Dutt, James Williams, Luqi Yuan, Midya Parto, Franco Nori, Shanhui Fan, and Alireza Marandi. Topological dissipation in a time-multiplexed photonic resonator network. *Nature Physics*, 18(4):442–449, 2022.
- [27] Goran Lindblad. On the generators of quantum dynamical semigroups. *Communications in mathematical physics*, 48(2):119–130, 1976.
- [28] Vittorio Gorini, Andrzej Kossakowski, and Ennackal Chandy George Sudarshan. Completely positive dynamical semigroups of n-level systems. *Journal of Mathematical Physics*, 17(5):821–825, 1976.
- [29] Andrzej Jamiolkowski. Linear transformations which preserve trace and positive semidefiniteness of operators. *Reports on Mathematical Physics*, 3:275–278, 1972.
- [30] Tony E. Lee. Anomalous edge state in a non-hermitian lattice. *Phys. Rev. Lett.*, 116:133903, Apr 2016.
- [31] Yong Xu, Sheng-Tao Wang, and L.-M. Duan. Weyl exceptional rings in a three-dimensional dissipative cold atomic gas. *Phys. Rev. Lett.*, 118:045701, Jan 2017.
- [32] Yu Chen and Hui Zhai. Hall conductance of a non-hermitian chern insulator. *Phys. Rev. B*, 98:245130, Dec 2018.
- [33] Huitao Shen, Bo Zhen, and Liang Fu. Topological band theory for non-hermitian hamiltonians. *Phys. Rev. Lett.*, 120:146402, Apr 2018.
- [34] Shunyu Yao and Zhong Wang. Edge states and topological invariants of non-hermitian systems. *Phys. Rev. Lett.*, 121:086803, Aug 2018.
- [35] Shunyu Yao, Fei Song, and Zhong Wang. Non-hermitian chern bands. *Phys. Rev. Lett.*, 121:136802, Sep 2018.
- [36] Masaya Nakagawa, Norio Kawakami, and Masahito Ueda. Non-hermitian kondo effect in ultracold alkaline-earth atoms. *Phys. Rev. Lett.*, 121:203001, Nov 2018.
- [37] Kazuki Yokomizo and Shuichi Murakami. Non-bloch band theory of non-hermitian systems. *Phys. Rev. Lett.*, 123:066404, Aug 2019.
- [38] Kohei Kawabata, Ken Shiozaki, Masahito Ueda, and Masatoshi Sato. Symmetry and topology in non-hermitian physics. *Phys. Rev. X*, 9:041015, Oct 2019.
- [39] Fei Song, Shunyu Yao, and Zhong Wang. Non-hermitian skin effect and chiral damping in open quantum systems. *Phys. Rev. Lett.*, 123:170401, Oct 2019.
- [40] Takumi Bessho and Masatoshi Sato. Nielsen-ninomiya theorem with bulk topology: Duality in floquet and non-hermitian systems. *Phys. Rev. Lett.*, 127:196404, Nov 2021.
- [41] Kun Ding, Chen Fang, and Guancong Ma. Non-hermitian topology and exceptional-point geometries. *Nature Reviews Physics*, 4(12):745–760, 2022.
- [42] Zongping Gong Yuto Ashida and Masahito Ueda. Non-hermitian physics. *Advances in Physics*, 69(3):249–435, 2020.
- [43] Alexandre Chaduteau, Derek K. K. Lee, and Frank Schindler. Lindbladian versus postselected non-hermitian topology. *Phys. Rev. Lett.*, 136:016603, Jan 2026.

- [44] Huixia Gao, Konghao Sun, Dengke Qu, Kunkun Wang, Lei Xiao, Wei Yi, and Peng Xue. Photonic chiral state transfer near the liouvillian exceptional point. *Phys. Rev. Lett.*, 134:146602, Apr 2025.
- [45] Yan He and Chih-Chun Chien. Uhlmann holonomy against lindblad dynamics of topological systems at finite temperatures. *Phys. Rev. B*, 106:024310, Jul 2022.
- [46] C-E Bardyn, M A Baranov, C V Kraus, E Rico, A İmamoğlu, P Zoller, and S Diehl. Topology by dissipation. *New Journal of Physics*, 15(8):085001, 2013.
- [47] Charles-Edouard Bardyn, Lukas Wawer, Alexander Altland, Michael Fleischhauer, and Sebastian Diehl. Probing the topology of density matrices. *Phys. Rev. X*, 8:011035, Feb 2018.
- [48] Liang Mao, Fan Yang, and Hui Zhai. Symmetry-preserving quadratic lindbladian and dissipation driven topological transitions in gaussian states. *Reports on Progress in Physics*, 87(7):070501, jun 2024.
- [49] Wenzhi Wang and Wei Yi. Dynamic transition of the density-matrix topology under parity-time symmetry. *Phys. Rev. B*, 110:155141, Oct 2024.
- [50] Zhan Gao and Yan He. Quantum quench dynamics of berry and uhlmann phases in topological systems. *Phys. Rev. B*, 108:085126, Aug 2023.
- [51] Marcos Atala, Monika Aidelsburger, Julio T. Barreiro, Dmitry Abanin, Takuya Kitagawa, Eugene Demler, and Immanuel Bloch. Direct measurement of the zak phase in topological bloch bands. *Nature Physics*, 9(12):795–800, 2013.
- [52] Hirokazu Miyake, Georgios A. Siviloglou, Colin J. Kennedy, William Cody Burton, and Wolfgang Ketterle. Realizing the harper hamiltonian with laser-assisted tunneling in optical lattices. *Phys. Rev. Lett.*, 111:185302, Oct 2013.
- [53] M. Aidelsburger, M. Atala, M. Lohse, J. T. Barreiro, B. Paredes, and I. Bloch. Realization of the hofstadter hamiltonian with ultracold atoms in optical lattices. *Phys. Rev. Lett.*, 111:185301, Oct 2013.
- [54] E. Alba, X. Fernandez-Gonzalvo, J. Mur-Petit, J. K. Pachos, and J. J. Garcia-Ripoll. Seeing topological order in time-of-flight measurements. *Phys. Rev. Lett.*, 107:235301, Nov 2011.
- [55] Philipp Hauke, Maciej Lewenstein, and André Eckardt. Tomography of band insulators from quench dynamics. *Phys. Rev. Lett.*, 113:045303, Jul 2014.
- [56] N. Fläschner, B. S. Rem, M. Tarnowski, D. Vogel, D.-S. Lühmann, K. Sengstock, and C. Weitenberg. Experimental reconstruction of the berry curvature in a floquet bloch band. *Science*, 352(6289):1091–1094, 2016.
- [57] Tracy Li, Lucia Duca, Martin Reitter, Fabian Grusdt, Eugene Demler, Manuel Endres, Monika Schleier-Smith, Immanuel Bloch, and Ulrich Schneider. Bloch state tomography using wilson lines. *Science*, 352(6289):1094–1097, 2016.